ICES REPORT 15-02

January 2015

Adaptive Surrogate Modeling for Response of Surface Approximations with Application to Bayesian Interference

by

Serge Prudhomme an Corey M. Bryant

The Institute for Computational Engineering and Sciences
The University of Texas at Austin
Austin, Texas 78712

Reference: Serge Prudhomme an Corey M. Bryant, "Adaptive Surrogate Modeling for Response of Surface Approximations with Application to Bayesian Interference," ICES REPORT 15-02, The Institute for Computational Engineering and Sciences, The University of Texas at Austin, January 2015.

RESEARCH

Adaptive Surrogate Modeling for Response Surface Approximations with Application to Bayesian Inference

Serge Prudhomme[1*] and Corey M Bryant[2]

*Correspondence:
serge.prudhomme@polymtl.ca
[1]Département de Mathématiques et de Génie Industriel, Ecole Polytechnique de Montréal, Montréal, Québec, Canada
Full list of author information is available at the end of the article

Abstract

Parameter estimation for complex models using Bayesian inference is usually a very costly process as it requires a large number of solves of the forward problem. We propose here an approach to reduce the computational cost by constructing surrogate models that provide approximations of the true solutions of the forward problem. The surrogate models are built in an adaptive manner using a posteriori error estimates for quantities of interest in order to control their accuracy. Effectiveness of the proposed methodology is demonstrated on a numerical example dealing with the parameter calibration of the Spalart-Allmaras model for the simulation of turbulent channel flows.

Keywords: Goal-oriented error estimation, adjoint problem, turbulence modeling, Spalart-Allmaras model, parameter identification

1 Introduction

A general issue in parameter estimation using Bayesian inference is that one has to sample the forward model a very large number of times in order to obtain accurate posterior distributions of the parameters. In the case of complex models involving many parameters, the process often results in computational costs that far exceed computer resources currently available. Kennedy and O'Hagan [1] suggested to consider emulators of response surfaces in order to reduce the number of forward simulations and showed that it could lead to considerable computational savings. A variety of reduced models to estimate the likelihood function have since then been proposed in the literature [2, 3, 4, 5]. However, reduced models only provide approximations of the true solution and the accuracy of the response needs to be verified in order to obtain meaningful results.

We propose in this work to develop a goal-oriented error estimation procedure to adaptively construct reduced models, also referred to as surrogate models, of the Reynolds averaged Navier-Stokes (RANS) models for the simulation of turbulent flows. Goal-oriented error estimation was initially designed as an adjoint-based method to estimate discretization errors in finite element solutions of boundary-value problems with respect to quantities of interest. The method was later extended to the estimation and control of modeling error when a fine scale model is replaced by a coarse-scale model [6, 7]. The goal-oriented error estimation framework will be used here not only to assess the accuracy of the surrogate models but also to guide the adaptive process for improving the representation of the true response provided by the reduced model.

We illustrate the methodology on examples concerning the simulation of turbulent channel flows. Turbulence will be modeled here by the Reynolds averaged Navier-Stokes (RANS) equations, supplemented by the Spalart-Allmaras model for the description of the Reynolds stress. This closure model involves several parameters that need to be calibrated in order to be useful. Values of the parameters have been proposed in [8, 9, 10]. Even though the turbulence community is well aware that the closure model parameters may include some level of uncertainty, rigorous quantification of these uncertainties has seldom been analyzed in the computational fluid dynamics literature, with the exception, maybe, of [11, 10] where the application of Bayesian inference is used to quantify uncertainties in simulations of turbulence. In the present study, our objective will be to reproduce some of the numerical examples described in [10] in order to demonstrate that one can confidently use reduced models rather than the full models to estimate the parameters of the Spalart-Allmaras model.

The paper is organized as follows: following the introduction, we describe in Section 2 the model problem, namely the Reynolds averaged Navier-Stokes equations and the Spalart-Allmaras model for the Reynolds stress, and derive the weak formulation of the deterministic problem. We briefly recall in Section 3 some concepts of probability theory and present the parameterized reduced model. We describe in Section 4 the goal-oriented error estimation and adaptivity methodology for the construction of the reduced model. We finally apply the methodology to Bayesian inference and present some numerical results in Section 5 before providing concluding remarks in Section 6.

2 Model problem

Let $\Omega \subset \mathbb{R}^3$ be the domain occupying the channel with boundary $\partial\Omega$. The RANS equations are derived from the Navier-Stokes equations using the Reynolds decomposition of the velocity, $\boldsymbol{u} = \boldsymbol{U} + \boldsymbol{u}'$, where $\boldsymbol{U} = \overline{\boldsymbol{u}}$ is the time-averaged velocity over a time interval $(0, T)$ and $\boldsymbol{u}'$ is the fluctuation about the mean. Substituting this decomposition into the Navier-Stokes equations and taking the average over $(0, T)$, we obtain the so-called RANS equations,

$$\begin{aligned} \frac{\partial U_i}{\partial t} + U_j \frac{\partial U_i}{\partial x_j} &= -\frac{1}{\rho}\frac{\partial P}{\partial x_i} + \frac{\partial}{\partial x_j}\left(\nu \frac{\partial U_i}{\partial x_j} - \overline{u_i' u_j'}\right), \quad \text{in } \Omega \\ \frac{\partial U_i}{\partial x_i} &= 0, \qquad \text{in } \Omega \end{aligned} \tag{1}$$

where P, ρ, and ν, denote the mean pressure, the density, and the kinematic viscosity, respectively. In order to be able to solve the equations, one usually considers a closure model for the Reynolds stress tensor $r_{ij} := \overline{u_i' u_j'}$ (scaled here by the constant density ρ) based on the eddy viscosity assumption. That is, the Reynolds stress is expressed as the viscosity term,

$$r_{ij} = -\nu_T \left(\frac{\partial U_i}{\partial x_j} + \frac{\partial U_j}{\partial x_i}\right), \tag{2}$$

where the "eddy viscosity" ν_T can be written in terms of a turbulent length and time scale. The practice of modeling the turbulence effects as a viscosity is motivated by

the fact that turbulence transports momentum in a similar manner to viscosity [12, 13, 14].

Many closure models have been proposed based on the eddy viscosity assumption, see e.g. [8, 15, 16, 17, 12, 9], some of which have been examined in the study by Oliver and Moser [10]. Here we will focus on one of the most commonly used models, the eddy viscosity transport model of Spalart and Allmaras [9]. The form considered in this work, as well as in [10], has been modified to avoid negative values of turbulent production and to ignore the transition to turbulence from a laminar initial condition. See [8, 18] for more details on the modified form of the model.

Starting from the eddy viscosity assumption (2), the Spalart-Allmaras model introduces a working variable $\tilde{\nu}$ such that

$$\nu_T = \tilde{\nu} f_{v1}, \tag{3}$$

where

$$f_{v1} = \frac{\chi^3}{\chi^3 + c_{v1}^3}, \qquad \chi = \frac{\tilde{\nu}}{\nu}. \tag{4}$$

The working variable is taken to be governed by the transport equation

$$\frac{D\tilde{\nu}}{Dt} = c_{b1}\tilde{S}\tilde{\nu} - c_{w1} f_w \left(\frac{\tilde{\nu}}{d}\right)^2 + \frac{1}{\sigma_{\mathrm{SA}}}\left[\frac{\partial}{\partial x_j}\left((\nu + \tilde{\nu})\frac{\partial \tilde{\nu}}{\partial x_j}\right) + c_{b2}\frac{\partial \tilde{\nu}}{\partial x_j}\frac{\partial \tilde{\nu}}{\partial x_j}\right], \tag{5}$$

where d is the distance to the nearest wall and parameter c_{w1} is defined as:

$$c_{w1} = \frac{c_{b1}}{\kappa^2} + \frac{1 + c_{b2}}{\sigma_{\mathrm{SA}}}. \tag{6}$$

The remaining undefined terms are given by the following relationships,

$$\tilde{S} = \begin{cases} S + \bar{S}, & \bar{S} \geq -c_{v2} S, \\ S + \dfrac{S(c_{v2}^2 S + c_{v3}\bar{S})}{(c_{v3} - 2c_{v2})S - \bar{S}}, & \bar{S} < -c_{v2} S, \end{cases} \tag{7}$$

where S is the magnitude of the vorticity, and

$$\bar{S} = \frac{\tilde{\nu}}{\kappa^2 d^2} f_{v2}, \qquad f_{v2} = 1 - \frac{\chi}{1 + \chi f_{v1}}, \tag{8}$$

$$f_w = g\left(\frac{1 + c_{w3}^6}{g^6 + c_{w3}^6}\right)^{1/6}, \quad g = r + c_{w2}(r^6 - r), \quad r = \frac{\tilde{\nu}}{\tilde{S}\kappa^2 d^2}. \tag{9}$$

The values of the parameters c_{b1}, σ_{SA}, c_{b2}, κ, c_{w2}, c_{w3}, c_{v1}, c_{v2}, and c_{v3}, suggested by Spalart and Allmaras, are provided in Table 1.

We suppose that our primary goal is the prediction of the centerline velocity in a fully-developed incompressible channel flow at $Re_\tau = 5000$. The turbulence is assumed non-homogeneous in the y-direction (wall normal direction) but homogeneous in the x-direction, reducing the complexity of the RANS equations significantly. Derivatives of statistical variables are all assumed to vanish with respect to

x and t, except the mean pressure gradient in the x-direction, as it serves as the driving force for the flow [12]. Thus, $U_2 = 0$, and $U_1 = U(y)$ is only a function of y, so that the mean flow equations reduce to

$$0 = -\frac{1}{\rho}\frac{\partial P}{\partial x} + \frac{\partial}{\partial y}\left(\nu\frac{\partial U}{\partial y} - \overline{u'_x u'_y}\right), \qquad \text{in } \Omega, \tag{10}$$

$$0 = -\frac{1}{\rho}\frac{\partial P}{\partial y} - \frac{\partial}{\partial y}\left(-\overline{u'_x u'_y}\right), \qquad \text{in } \Omega. \tag{11}$$

Using the fact that $\partial_x(\overline{u'_x u'_y}) = 0$, we can differentiate the second equation with respect to x to show that $\partial_y \partial_x P = 0$ and, thus, the gradient of P is constant [12]. To simplify the presentation, we set $1/\rho\ \partial_x P = 1$ and control the dynamics of the flow purely through the Reynolds number.

Let $D = (0, H)$, where H represents the half height of the channel. Combining the simplified form of the RANS equations with the Spalart-Allmaras turbulence model, the strong form of the equations now reads:

$$1 = \frac{\partial}{\partial y}\left((\nu + \nu_T)\frac{\partial U}{\partial y}\right), \quad y \in D, \tag{12}$$

$$\begin{aligned} 0 = c_{b1}\tilde{S}\tilde{\nu} - c_{w1} f_w \left(\frac{\tilde{\nu}}{y}\right)^2 \\ + \frac{1}{\sigma_{\mathrm{SA}}}\frac{\partial}{\partial y}\left[\left((\nu + \tilde{\nu})\frac{\partial \tilde{\nu}}{\partial y}\right) + c_{b2}\left(\frac{\partial \tilde{\nu}}{\partial y}\right)^2\right], \quad y \in D. \end{aligned} \tag{13}$$

Equation (12) represents the RANS momentum equation, which governs the behavior of the flow variable U; Equation (13) is the transport equation for the Spalart-Allmaras working variable $\tilde{\nu}$. The equations are supplemented with the boundary conditions:

$$\begin{aligned} &U(0) = 0, \quad \partial_y U(H) = 0, \\ &\tilde{\nu}(0) = 0, \quad \partial_y \tilde{\nu}(H) = 0, \end{aligned} \tag{14}$$

which amount to symmetry boundary conditions at the center of the channel ($\partial_y U(H) = 0$ and $\partial_y \tilde{\nu}(H) = 0$) and no slip conditions at the walls. We indeed assume that the eddy viscosity is symmetric across the channel and vanishes at the wall.

The weak formulation of the problem is derived in the typical manner of multiplying Equations (12) and (13) by suitable test functions and integrating by parts. Let $\mathcal{V} = V \times V$ where $V = \{v \in H^1(D) |\ v(0) = 0\}$. Then the problem becomes:

$$\begin{aligned} &\text{Find } (U, \tilde{\nu}) \in \mathcal{V} \text{ such that} \\ &\quad \mathcal{B}\left((U, \tilde{\nu}); (v_u, v_{\tilde{\nu}})\right) = \mathcal{F}\left((v_U, v_{\tilde{\nu}})\right), \quad \forall (v_U, v_{\tilde{\nu}}) \in \mathcal{V}, \end{aligned} \tag{15}$$

where

$$\mathcal{F}\left((v_U, v_{\tilde{\nu}})\right) = \int_0^H v_U dy \tag{16}$$

$$\mathcal{B}\left((U,\tilde{\nu});(v_U,v_{\tilde{\nu}})\right) = \mathcal{B}_m\left((U,\tilde{\nu});(v_U,v_{\tilde{\nu}})\right) + \mathcal{B}_t\left((U,\tilde{\nu});(v_U,v_{\tilde{\nu}})\right), \tag{17}$$

with

$$\mathcal{B}_m\left((U,\tilde{\nu});(v_U,v_{\tilde{\nu}})\right) = -\int_0^H \left((\nu+\nu_T)\frac{\partial U}{\partial y}\right)\frac{\partial v_U}{\partial y}\; dy, \tag{18}$$

$$\begin{aligned}\mathcal{B}_t\left((U,\tilde{\nu});(v_U,v_{\tilde{\nu}})\right) = \int_0^H &\left[c_{b1}\tilde{S}\tilde{\nu} - c_{w1}f_w\left(\frac{\tilde{\nu}}{y}\right)^2\right]v_{\tilde{\nu}} \\ &- \frac{1}{\sigma_{\mathrm{SA}}}\left[\left((\nu+\tilde{\nu})\frac{\partial\tilde{\nu}}{\partial y}\right) + c_{b2}\left(\frac{\partial\tilde{\nu}}{\partial y}\right)^2\right]\frac{\partial v_{\tilde{\nu}}}{\partial y}\; dy.\end{aligned} \tag{19}$$

The above equations will be solved using a standard continuous finite element discretization on D. Let $\mathcal{V}^h \subset \mathcal{V}$ be the finite element subspace consisting of piecewise linear functions, on a suitable partition of D with maximal element diameter h. Given a set of parameter values, the finite element approximation of (15) is given by,

$$\begin{aligned}&\text{Find } (U^h,\tilde{\nu}^h) \in \mathcal{V}^h \text{ such that} \\ &\quad \mathcal{B}\left((U^h,\tilde{\nu}^h);(v_u,v_{\tilde{\nu}})\right) = \mathcal{F}\left((v_U,v_{\tilde{\nu}})\right), \quad \forall (v_U,v_{\tilde{\nu}}) \in \mathcal{V}^h.\end{aligned} \tag{20}$$

A computable system of equations can then be obtained using Newton's method, linearizing about the approximate state $(U^h,\tilde{\nu}^h)$.

Problem (20) represents the model problem we shall consider throughout this work. However, since the RANS turbulence model parameters are uncertain, these equations need to be parameterized by random variables; we discuss the characterizations of the uncertain parameters in the following section.

3 Uncertainty characterization and reduced model

As previously discussed, the parameters of the Spalart-Allmaras turbulence model (3) and (5) are usually assumed constant with the values provided in Table 1. In this work, we suppose that a subset of these parameters are in fact unknown, or random. Therefore, the boundary-value problem can be viewed as parameterized by these uncertain coefficients.

We briefly review some relevant concepts of probability theory and the use of polynomial expansions, commonly referred to as generalized polynomial chaos, to represent the effects of uncertainty in the model response.

Let $\{\Theta,\Sigma,P\}$ be a probability space, where Θ is the sample space of random events, Σ is a σ-algebra, and P is the probability measure on Σ, meaning $P(\Theta)=1$. A random variable on the probability space is defined as a P-measurable function of Θ. Let $\Xi \subset \mathbb{R}^n$. We use the notation $\boldsymbol{\xi}:\Theta\to\Xi$ to denote a random variable and denote by p_ξ the associated probability density function.

Introducing the notion of random variables into the boundary-value problem implies that the solution u is a random process. We will consider the differential equations to be parameterized by $\boldsymbol{\xi}$. Let $\mathcal{V}^h$ be as defined above; then, Problem (20) can

be rewritten as,

$$\begin{aligned} &\text{Find } (U^h(\cdot,\boldsymbol{\xi}),\tilde{\nu}^h(\cdot,\boldsymbol{\xi})) \in \mathcal{V}^h \text{ such that} \\ &\quad \mathcal{B}_{\boldsymbol{\xi}}\left((U^h,\tilde{\nu}^h);(v_u,v_{\tilde{\nu}})\right) = \mathcal{F}_{\boldsymbol{\xi}}\left((v_U,v_{\tilde{\nu}})\right), \quad \forall (v_U,v_{\tilde{\nu}}) \in \mathcal{V}^h, \end{aligned} \tag{21}$$

where the subscript $\boldsymbol{\xi}$ is used to indicate the dependence on the parameter.

At this point, the solution to (21) represents a semi-discrete solution, being continuously dependent on the random variable $\boldsymbol{\xi}$. To discretize the solution in terms of the random variable, many authors have proposed the use of generalized polynomial chaos [19, 20, 21, 22, 23, 24, 25], led by the seminal work of Ghanem and Spanos [20].

Let $\alpha = (\alpha_1, \ldots, \alpha_n) \in \mathbb{N}^n$ be a multi-index and let $\Psi_\alpha(\boldsymbol{\xi})$ denote the (multivariate) polynomials

$$\Psi_\alpha(\boldsymbol{\xi}) = \psi_{\alpha_1}(\xi_1)\cdots\psi_{\alpha_n}(\xi_n), \tag{22}$$

where the univariate polynomial $\psi_{\alpha_i}(\xi_i)$ is the orthonormal polynomial of degree α_i with respect to the probability distribution of ξ_i [26, 27, 28]. That is, for $\alpha, \beta \in \mathbb{N}^n$,

$$\int_\Omega \Psi_\alpha(\boldsymbol{\xi})\Psi_\beta(\boldsymbol{\xi})p_{\boldsymbol{\xi}}(\boldsymbol{\xi})d\boldsymbol{\xi} = \delta_{\alpha\beta}, \tag{23}$$

where $\delta_{\alpha\beta}$ is the Kronecker delta:

$$\delta_{\alpha\beta} = \begin{cases} 1, & \alpha_i = \beta_i,\ i = 1,\ldots,n \\ 0, & \text{otherwise.} \end{cases} \tag{24}$$

Then, for any $Z \in L^2(\Theta,\Sigma,P)$, the generalized polynomial chaos expansion,

$$Z^N = \sum_{\alpha\in\mathbb{N}^n} z_\alpha \Psi_\alpha(\boldsymbol{\xi}), \qquad z_\alpha = \langle Z, \Psi_\alpha \rangle, \tag{25}$$

converges to Z in mean square sense.

Convergence of polynomial expansions of this type for square integrable functions on Θ is established by generalizations of the Cameron-Martin Theorem [29, 30]. In this work, we use uniform random variables to describe the uncertain parameters, which means that the basis is given in terms of Legendre polynomials [21, 31].

A number of methods for computing the coefficients of the expansion have been developed and generally fall into two categories: intrusive and non-intrusive. Non-intrusive approaches attempt to estimate the coefficients of a generalized polynomial chaos expansion by solving the deterministic problem at a set of realizations of $\boldsymbol{\xi}$. As a result, existing simulation codes can usually be used directly. In contrast, intrusive approaches, such as those based on Galerkin methods, solve a system of equations for the entire set of expansion coefficients; typically this requires the use of specially designed solvers. We shall focus on non-intrusive approaches here since they allow for the existing turbulence simulation codes to be used with minimal modification. Moreover, the set of independent parameter values can usually be run

in parallel, making non-intrusive approaches more efficient. The error estimates and decomposition strategy introduced in the next section are rather general and can be utilized with most intrusive or non-intrusive surrogate methods for uncertainty quantification [32, 33, 25]. However, for completeness, we detail the pseudo-spectral projection method [31] used in the present work.

In order to represent the solution U^h of (21) by its generalized polynomial chaos expansion, it remains to calculate the coefficients. The coefficients are determined by the projection of the solution onto the basis, i.e.

$$U^h_\alpha(y) = \left\langle U^h, \Psi_\alpha \right\rangle := \int_\Xi U^h(y, \boldsymbol{\xi}) \Psi_\alpha(\boldsymbol{\xi}) p_\xi(\boldsymbol{\xi}) d\boldsymbol{\xi}. \tag{26}$$

where Ψ_α are the orthogonal polynomials associated with the distribution of $\boldsymbol{\xi}$.

As discussed previously, non-intrusive approaches aim to compute the coefficients of the expansion based on independent realizations of the deterministic solution $u(y, \boldsymbol{\xi})$. One can use sampling-based methods, such as Monte Carlo or Latin hypercube sampling, to estimate the integral in (26). In high-dimensional parameter spaces sampling may be preferred, since convergence is based on the number of samples and not the dimension of the space. In our case, the dimension will remain relatively low so that we can rely on direct numerical integration using quadrature techniques. Even in a high number of dimensions authors have proposed the use of sparse representations to make the process more efficient [34, 25, 35, 36, 37, 38, 39].

Using basic quadrature formula we can approximate the integration in (26) by,

$$U^h_\alpha(y) \approx \sum_{k=1}^{m} U^h(y, \boldsymbol{\xi}^k) \Psi_\alpha(\boldsymbol{\xi}^k) w^k, \tag{27}$$

where $\{\boldsymbol{\xi}^k\}$ and $\{w^k\}$ are quadrature points and weights, respectively. It has been shown in [40] that using a Gaussian quadrature rule yields a geometric convergence rate; it does however require a number of quadrature points $m(N)$ that scales exponentially with the dimension of Ξ.

Finally, we can represent the fully discretized solution to (21) as

$$U^{h,N}(y, \boldsymbol{\xi}) = \sum_{\alpha=0}^{N} U^h_\alpha(y) \Psi_\alpha(\boldsymbol{\xi}), \tag{28}$$

where $U^h_\alpha(y) \in V^h \subset V$, $\forall \alpha = 1, \ldots, N$ are computed independently using (27).

The fully discretized solution $U^{h.N}$, together with $\tilde{\nu}^{h,N}$, having finite length expansions, represent a reduced model for the semi-discrete solution $(U^h, \tilde{\nu})$. Selection of which terms, or polynomial bases, to include in the expansion will be driven by the adaptive procedure presented in the following section.

4 Goal-oriented adaptive surrogate modeling

In this section, we provide details of the error estimation and adaptive procedure for boundary-value problems parameterized by uncertainty. First we review goal-oriented error estimation in the deterministic setting. We then demonstrate the extension to the case of uncertainty as proposed in previous works [41, 42, 43, 32,

33, 31, 44]. In addition we suggest an adaptive procedure based on the contribution of higher-order expansion terms to the error in the quantity of interest. Finally we present results from the application of the procedure to the model problem of Section 2.

4.1 Goal-oriented error estimation: deterministic setting

Since its introduction in the 1990's [45, 46, 47, 48], goal-oriented error estimation has grown in popularity in the finite element community. Here we only provide a brief outline of the approach and refer the interested reader to more extensive descriptions and reviews of the methodology [49, 50, 48, 51].

In order to derive the error estimation and adaptive strategy, we first require the definition of a linear functional of the solution representing a quantity of interest. We will use the average of the mean flow velocity U over the channel cross-section,

$$\mathcal{Q}\left((U,\tilde{\nu})\right) = \int_0^H U \; dy. \tag{29}$$

Since the velocity profile is expected to reach the maximum at the center of the channel, this quantity of interest will be more sensitive to the centerline velocity.

The core ingredient of the goal-oriented framework is the so-called adjoint problem, which seeks a generalized Green's function associated with the quantity of interest. In the case of a nonlinear operator, such as (20), the linearized operator is used to define the adjoint equation [49, 47, 52, 53, 51]. For our model problem that means that the adjoint equation is given by,

$$\begin{aligned} &\text{Find } (z_U, z_{\tilde{\nu}}) \in \mathcal{V} \text{ such that} \\ &\qquad \mathcal{B}'\left((U,\tilde{\nu});(z_U,z_{\tilde{\nu}}),(v_U,v_{\tilde{\nu}})\right) = \mathcal{Q}\left((v_U,v_{\tilde{\nu}})\right), \quad \forall (v_U,v_{\tilde{\nu}}) \in \mathcal{V}, \end{aligned} \tag{30}$$

where the operator $\mathcal{B}^{'}$ used to compute updates in Newton's method for solving the nonlinear primal problem (20). The definition of the adjoint equation allows one to establish a computable estimate for the error in the quantity of interest, $\mathcal{E}_{\mathcal{Q}} = \mathcal{Q}\left((U,\tilde{\nu})\right) - \mathcal{Q}\left((U^h,\tilde{\nu}^h)\right)$. Using the definition of the residual

$$\mathcal{R}\left((U^h,\tilde{\nu}^h);(z_U,z_{\tilde{\nu}})\right) := \mathcal{F}\left((z_U,z_{\tilde{\nu}})\right) - \mathcal{B}\left((U^h,\tilde{\nu}^h);(z_u,z_{\tilde{\nu}})\right), \tag{31}$$

we can write, introducing the errors in the solution as $e_U = U - U^h$ and $e_{\tilde{\nu}} = \tilde{\nu} - \tilde{\nu}^h$,

$$\begin{aligned} \mathcal{E}_{\mathcal{Q}} &= \mathcal{Q}\left((U,\tilde{\nu})\right) - \mathcal{Q}\left((U^h,\tilde{\nu}^h)\right) \\ &= \mathcal{Q}\left((e_U,e_{\tilde{\nu}})\right) && (32)\\ &= \mathcal{B}'\left((U,\tilde{\nu});(z_U,z_{\tilde{\nu}}),(e_U,e_{\tilde{\nu}})\right) && (33)\\ &= \mathcal{R}\left((U^h,\tilde{\nu}^h);(z_U,z_{\tilde{\nu}})\right) - \Delta_{\mathcal{B}}\left((U,\tilde{\nu}),(e_U,e_{\tilde{\nu}}),(z_U,z_{\tilde{\nu}})\right) && (34)\\ &= \mathcal{R}\left((U^h,\tilde{\nu}^h);(z_U-\phi_U^h,z_{\tilde{\nu}}-\phi_{\tilde{\nu}}^h)\right) - \Delta_{\mathcal{B}}\left((U,\tilde{\nu}),(e_U,e_{\tilde{\nu}}),(z_U,z_{\tilde{\nu}})\right), && (35) \end{aligned}$$

for all $(\phi_U^h,\phi_{\tilde{\nu}}^h) \in V^h$. Note that Equation (32) holds because of the linearity of $\mathcal{Q}$, that Equation (33) follows from using the adjoint problem, that Equation (34) is a consequence of the definition of the linearized operator $\mathcal{B}'$ and of the residual (31),

and that Equation (35) is a result of Galerkin orthogonality. Due to the complexity of estimating $\Delta_{\mathcal{B}}$, and the fact that it is deemed to be higher-order, the term is often neglected [47, 54, 55]. Incorporating the higher-order nonlinear term into an error estimation procedure is the focus of ongoing work [52]. Nevertheless, we proceed assuming that the contribution due to linearization is negligible.

Furthermore, the representation (35) cannot be used directly as it involves the exact adjoint solution $(z_U, z_{\tilde{\nu}})$. To obtain a computable estimate of the error in the quantity of interest, we instead introduce an approximate adjoint solution from an enriched finite element space $\mathcal{V}^+$ where $\mathcal{V}^h \subset \mathcal{V}^+ \subset \mathcal{V}$. That is,

$$\begin{aligned} &\text{Find } (z_U^+, z_{\tilde{\nu}}^+) \in \mathcal{V}^+ \text{ such that} \\ &\quad \mathcal{B}'\left((U^h, \tilde{\nu}^h); (z_U^+, z_{\tilde{\nu}}^+), (v_U, v_{\tilde{\nu}})\right) = \mathcal{Q}\left((v_U, v_{\tilde{\nu}})\right), \quad \forall (v_U, v_{\tilde{\nu}}) \in \mathcal{V}^+, \end{aligned} \tag{36}$$

where the enriched space will be taken as the space of piecewise quadratic functions on the same partition of D as V^h. Thus, a computable error estimate for the error in the quantity of interest is provided by

$$\begin{aligned} \mathcal{E}_{\mathcal{Q}} &= \mathcal{Q}\left((U, \tilde{\nu})\right) - \mathcal{Q}\left((U^h, \tilde{\nu}^h)\right) \\ &\approx \mathcal{R}\left((U^h, \tilde{\nu}^h); (z_U - \phi_U^h, z_{\tilde{\nu}} - \phi_{\tilde{\nu}}^h)\right) := \eta\left((U^h, \tilde{\nu}^h), (z_U^+, z_{\tilde{\nu}}^+)\right). \end{aligned} \tag{37}$$

In addition, η can be broken into elementwise contributions to define refinement indicators for mesh adaptation.

4.2 Goal-oriented error estimation: uncertainty setting

We next turn our focus to the extension of the deterministic goal-oriented error estimation to the case of boundary-value problems with uncertainty. First we establish an estimate of the overall accuracy of the surrogate solution $U^{h,N}$ in terms of the quantity of interest and then suggest a procedure to adapt the surrogate expansion based on indicators derived from this estimate.

To measure the error in the response of the quantity of interest over the range of parameters $\boldsymbol{\xi}$, we use the L_2 norm of the 'deterministic' error,

$$\left\| \mathcal{Q}\left((U, \tilde{\nu})\right) - \mathcal{Q}\left((U^{h,N}, \tilde{\nu}^{h,N})\right) \right\|_{L_2(\Xi)}. \tag{38}$$

This metric is actually a natural choice as it implies the control of the mean and standard deviation of the error.

The first step in extending the deterministic results to the error (38) is to establish the same type of error representation for $\mathcal{Q}\left((U, \tilde{\nu})\right) - \mathcal{Q}\left((U^{h,N}, \tilde{\nu}^{h,N})\right)$. To do so, we define the adjoint equation in terms of the surrogate $U^{h,N}$,

$$\begin{aligned} &\text{Find } (\hat{z}_U, \hat{z}_{\tilde{\nu}}) \in \mathcal{V} \text{ such that} \\ &\quad \mathcal{B}'\left((U^{h,N}, \tilde{\nu}^{h,N}); (\hat{z}_U, \hat{z}_{\tilde{\nu}}), (v_U, v_{\tilde{\nu}})\right) = \mathcal{Q}\left((v_U, v_{\tilde{\nu}})\right), \quad \forall (v_U, v_{\tilde{\nu}}) \in \mathcal{V}. \end{aligned} \tag{39}$$

Since $U^{h,N} \in \mathcal{V}$ for any choice of $\boldsymbol{\xi}$ we can work through the same procedure as for the deterministic procedure to arrive at,

$$\mathcal{E}_{\mathcal{Q}} = \mathcal{Q}\left((U,\tilde{\nu})\right) - \mathcal{Q}\left((U^{h,N},\tilde{\nu}^{h,N})\right) = \mathcal{R}\left((U^{h,N},\tilde{\nu}^{h,N});(\hat{z}_U,\hat{z}_{\tilde{\nu}})\right) - \Delta_{\mathcal{B}}\left((U,\tilde{\nu}),(e_U,e_{\tilde{\nu}}),(\hat{z}_U,\hat{z}_{\tilde{\nu}})\right). \tag{40}$$

The idea is then to obtain an approximation of $\mathcal{R}\left((U^{h,N},\tilde{\nu}^{h,N});(\hat{z}_U,\hat{z}_{\tilde{\nu}})\right)$ in the same way as before using a discrete adjoint solution $(\hat{z}_U^+,\hat{z}_{\tilde{\nu}}^+) \in V^+$.

The other key to obtaining a tractable estimator for (38) is the evaluation of the norm itself. Since evaluating the norm involves more integration in a possibly high-dimensional parameter space we will likely need to evaluate the error representation in a manner that scales exponentially with the parameter dimension. For each quadrature point (40), one requires the solution of the adjoint equation (39), a process that would quickly become prohibitively expensive. Instead, we propose to construct a reduced model of the semi-discrete adjoint solution, which can then be evaluated with minimal cost at any point in parameter space. Let

$$\hat{z}^{+,N}(y,\boldsymbol{\xi}) = \sum_{\alpha=0}^{N} \hat{z}_\alpha^+(y)\Psi_\alpha(\boldsymbol{\xi}), \tag{41}$$

where $z_\alpha^+(y) \in V^+ \subset V$, $\forall \alpha = 1,\ldots,N$ are computed in the same way as the forward solution, c.f. Equation (27). With these two additional modifications, we then have a computable estimate for the error (38), as established in the following theorem.

Theorem 4.1 *Assume $B_{\boldsymbol{\xi}}$ to be continuously differentiable, for any $\boldsymbol{\xi} \in \Xi$, in a subset of $\mathcal{V}$ that contains $(U,\tilde{\nu})$, $(U^h,\tilde{\nu}^h)$, $(U^{h,N},\tilde{\nu}^{h,N})$. Let $(\hat{z}_U^{+,N},\hat{z}_{\tilde{\nu}}^{+,N})$ be an approximation of the adjoint solution according to* (41)*. The error estimate*

$$\eta = \left\| \mathcal{R}_{\boldsymbol{\xi}}\left(\left(U^{h,N},\tilde{\nu}^{h,N}\right);\left(\hat{z}_U^{+,N},\hat{z}_{\tilde{\nu}}^{+,N}\right)\right)\right\|_{L^2(\Xi)}, \tag{42}$$

for (38) *satisfies the bound,*

$$\begin{aligned}\left|\left\|\mathcal{Q}\left((U,\tilde{\nu})\right) - \mathcal{Q}\left((U^{h,N},\tilde{\nu}^{h,N})\right)\right\|_{L^2(\Xi)} - \eta\right| \\ \leq \mathcal{O}\left(\left\|\left\|\left(e_U^{h,N},e_{\tilde{\nu}}^{h,N}\right)\right\|_V \left\|\left(\hat{z}_U - \hat{z}_U^{+,N},\hat{z}_{\tilde{\nu}} - \hat{z}_{\tilde{\nu}}^{+,N}\right)\right\|_V\right\|_{L^2(\Xi)}\right) \\ + \mathcal{O}\left(\left\|\left\|\left(e_U^{h,N},e_{\tilde{\nu}}^{h,N}\right)\right\|_V^2\right\|_{L^2(\Xi)}\right).\end{aligned} \tag{43}$$

For a proof, see [42, 43, 52].

The extension of the goal-oriented error estimation framework to boundary-value problems with uncertain data simply means that uncertainty can be considered in complex physical problems using a reduced-order surrogate model since its accuracy can be assessed in terms of the quantity of interest. Even more valuable, much as in the case of deterministic goal-oriented error estimation, estimates can be used to drive adaptivity to improve the approximations further, as we discuss in the next section.

4.3 Adaptive surrogate modeling

One major disadvantage of using quadrature-based sampling strategies for surrogate construction is that the number of points required for a fixed expansion order grows exponentially with parameter dimension; this is commonly referred to as the *curse of dimensionality*.

A number of different approaches have been proposed to minimize the effect of the curse of dimensionality. For example, one may choose to alter the quadrature formula used in calculating the expansion coefficients; in the case a tensor product quadrature formula is employed, authors have suggested sparse quadrature grids that can reduce the number of evaluations necessary for the same level of accuracy [25, 56, 3, 37, 38, 39]. Alternatively, or in a combined manner, higher-order information can be used to identify the more influential parameters; instead of increasing the expansion order uniformly (isotropic refinement), one may then choose to improve the surrogate model by adding bases functions that only correspond to the most important parameters (anisotropic refinement).

While our proposed framework can be used with a sparse quadrature formula, we will restrict our discussion to full tensor product quadrature since an anisotropic refinement strategy is more valuable in that scenario. In contrast to existing techniques for using higher-order information to drive anisotropic surrogate refinement, which are often based on heuristic measures, our approach identifies the components associated with the error in the quantity of interest.

In order to identify the most influential modes in the expansion, we use the residual in the error estimate (42). Yet, to do so, we must be able to identify the parameters to which the residual is most sensitive. We propose the use of yet another surrogate model, this one for the residual term itself,

$$\mathcal{E}(\boldsymbol{\xi}) := \sum_{\alpha=0}^{M} \mathcal{R}_\alpha \Psi_\alpha(\boldsymbol{\xi}) \approx \mathcal{R}_{\boldsymbol{\xi}} \left((U^{h,N}, \tilde{\nu}^{h,N}); (\hat{z}_U^{+,N}, \hat{z}_{\tilde{\nu}}^{+,N}) \right), \tag{44}$$

with a higher order $M > N$. The coefficients in (44) are calculated based on the same type of quadrature used for the primal and adjoint surrogates,

$$\mathcal{R}_\alpha = \sum_{k=1}^{m} \mathcal{R}_{\boldsymbol{\xi}^k} \left((U^{h,N}, \tilde{\nu}^{h,N}); (\hat{z}_U^{+,N}, \hat{z}_{\tilde{\nu}}^{+,N}) \right) \Psi_\alpha(\boldsymbol{\xi}^k) w^k. \tag{45}$$

Since $(U^{h,N}, \tilde{\nu}^{h,N})$ and $(z_U^{+,N}, z_{\tilde{\nu}}^{+,N})$ have fewer terms in the expansion, the residual surrogate provides information about how the error in the quantity of interest influences the higher-order terms. The relative magnitudes of the coefficients in $\mathcal{E}$ provide a weighting of the most important parameter directions or, more specifically, which basis functions should be added to the solution expansions. To precisely define the refinement strategy, we need a generalization of the set of multi-indices; let

$$\mathcal{I}_{\mathcal{N}} = \{\alpha \in \mathbb{N}^n : \alpha_j \leq N_j, j = 1, \ldots, n\}, \tag{46}$$

where $\mathcal{N} = (N_1, \ldots, N_n)$ represents the maximum polynomial degree in each direction. Higher-order expansions of the error will now be obtained using $\mathcal{M} =$

$\mathcal{N} + \mathbf{1} = \{N_1 + 1, \ldots, N_n + 1\}$. Thus, we seek the coefficients of $\mathcal{E}(\boldsymbol{\xi})$ in (44) in the set $\mathcal{I}_\mathcal{M} \setminus \mathcal{I}_\mathcal{N}$ with the largest magnitude, which will be added to the index set $\mathcal{I}_\mathcal{N}$ for the subsequent adaptive step. Algorithm 1 describes the detailed refinement strategy.

Algorithm 1: Anisotropic p refinement in Ξ.

Construct $\mathcal{E}(\boldsymbol{\xi}) = \sum_{\alpha \in \mathcal{I}_\mathcal{M}} \mathcal{R}_{\boldsymbol{\xi}}(u_\alpha^{h,N}, \hat{z}_\alpha^{+,N}) \Psi_\alpha(\boldsymbol{\xi})$;
Set $\beta^* = \sum_{\alpha \in \mathcal{I}_\mathcal{M} \setminus \mathcal{I}_\mathcal{N}} |\mathcal{R}_{\boldsymbol{\xi}}(u_\alpha^{h,N}, \hat{z}_\alpha^{+,N})|$.;
For $\alpha \in \mathcal{I}_\mathcal{M} \setminus \mathcal{I}_\mathcal{N}$, sort $|\mathcal{R}_{\boldsymbol{\xi}}(u_\alpha^{h,N}, \hat{z}_\alpha^{+,N})|$ in decending order giving index $\mathcal{I}_\alpha$.;
Given $0 \leq \eta \leq 1$, set $\beta = 0$ and $i = 0$;
while $\beta < \eta \beta^*$ **do**
    Set $i = i + 1$ and $\alpha^* = \mathcal{I}_\alpha(i)$;
    Set $\beta = \beta + |\mathcal{R}_{\boldsymbol{\xi}}(u_{\alpha^*}^{h,N}, \hat{z}_{\alpha^*}^{+,N})|$;
    for $j = 1 \to n$ **do**
        if $\alpha_j^* > N_j$ **then**
            Increase polynomial order of approximation in component j, $N_j \leftarrow N_j + 1$;
        end
    end
end

4.4 Numerical results for turbulence model problem

Finally we are prepared to apply the adaptive surrogate refinement procedure to the model problem of RANS turbulence modeling for incompressible flows. We will consider the physical discretization as fixed and focus on the adaptive construction of a surrogate model for the Spalart-Allmaras turbulence model with six uncertain parameters: κ, c_{b1}, σ_{SA}, c_{b2}, c_{v1}, c_{w2}. To evaluate the surrogate model, we will use both the error estimates established in this section as well as simulations of the quantity of interest provided by the full model to further establish the accuracy of our error estimates.

As mentioned previously we will consider uniform distributions for all uncertain parameters. The exact descriptions will be based on the nominal values presented in Table 1 with a range from 50 to 150 percent of the corresponding value; for example $\kappa \sim \mathcal{U}(0.205, 0.615)$.

Starting with a constant, or $N = 0$, surrogate model, we performed 17 adaptive steps adding additional polynomials to the expansion according to Algorithm 1. Figure 1 shows the convergence of the error estimate for the surrogate model. Compared to uniform, or isotropic p-refinement, the anisotropic refinement of the surrogate model leads to significant improvement of the error for an equal number of forward model evaluations, roughly two orders of magnitude reduction. The progression of the expansion order is shown in Table 2. We observe that the initial refinements are associated with the κ and c_{v1} parameters, demonstrating that their values have the greatest influence on the quantity of interest. Following initial refinement of κ and c_{v1}, we also see a continued increase in the expansion order for κ, which we would expect to see since it has a significant impact on the flow velocity away from the wall where the velocity is higher and thus contributes more significantly to the quantity of interest. Refinements are suggested for all model parameters, though c_{b2} is only modeled linearly, suggesting that the gradient of the working variable $\tilde{\nu}$ does not have a notable impact on the average velocity. Ultimately, we expected to

see a greater expansion order for c_{v1} than the other model parameters besides κ. We believe that the positive correlation between κ and c_{v1}, seen in the posterior distributions discussed in [10], contributed to refinement of only one of the two parameters being sufficient to accurately estimate the quantity of interest.

From Figure 2 one can clearly see that the adaptive surrogate model is able to capture the general response of the quantity of interest over the range of uncertain parameters. Furthermore, the convergence of the error estimate suggests that the reduced model can be used in further studies without a significant loss in accuracy. One attractive use case is that of model validation since many techniques, particularly Bayesian methods, require repeated evaluations of the forward model for the quantity of interest. While the surrogate presented in this section is capable of producing accurate predictions of the quantity of interest, in order to be useful in a validation setting, the reduced model must also exhibit the same sensitivities as the full model. We investigate this issue in the next section based on a simplified version of the Bayesian uncertainty quantification study performed in [10].

5 Efficient Bayesian inference

To this point we have restricted the discussion to verification of the adaptive surrogate modeling technique we propose. Often the full model is yet still in need of validation against experimental observations. While a reduced model can certainly make validation studies more computationally feasible, the more pressing question is whether using the surrogate model in place of the full model will lead to the same conclusions on the model's validity.

Here, we will not present validation results themselves, but instead show that calibrating the previously constructed surrogate model produces nearly identical results for the unknown parameters, and thus exhibits the same sensitivity to the data. In turn this means that it is reasonable to use the surrogate model as a replacement for the full model in a calibration and validation procedure; even if only for identifying calibration parameters that can then be fed into the full model for validation checks.

As a basis for comparison we use the work of Oliver and Moser [10], where Bayesian methods were used to evaluate the validity of a number of turbulence models and discrepancies. To simplify the presentation here, we restrict our investigation to the Spalart-Allmaras model discussed previously and show results based on only one description of uncertainty, whereas the authors in [10] considered multiple turbulence models and four different uncertainty models. A more thorough comparison and evaluation of the surrogate model was performed in [52].

We first provide an overview of the Bayesian methodology and then discuss the calibration data and uncertainty model used before showing results for the surrogate model and comparisons against full model.

5.1 Bayesian model calibration

Bayes' Theorem is a fundamental result of statistics and probability. Relatively recently, it has been adapted toward parameter identification for complex mathematical models. The advantage of Bayesian inference for model calibration is that it provides for a distribution of probable parameter values instead of the one best

fitting parameter value obtained from traditional optimization procedures. Bayesian parameter identification can be interpreted as an update of the degree of belief in the parameters.

The solution of the Bayesian calibration procedure is the posterior pdf, or the conditional distribution of the model parameters given the observed data. Let $\boldsymbol{q} \in \mathbb{R}^n$ represent the vector of calibration data, or observations, and let $\boldsymbol{\xi} \in \Xi = \mathbb{R}^m$ be the random variable representing the model parameters we wish to calibrate. The prior distribution of the parameters is denoted by $p(\boldsymbol{\xi})$ and encapsulates the prior knowledge one has about the parameters independent of the calibration data. Bayes' Theorem then states that the posterior distribution, $p(\boldsymbol{\xi}|\boldsymbol{q})$ is proportional to the prior times the likelihood $L(\boldsymbol{\xi}, \boldsymbol{q})$ of observing the data [57, 58],

$$p(\boldsymbol{\xi}|\boldsymbol{q}) = \frac{L(\boldsymbol{\xi}|\boldsymbol{q})\ p(\boldsymbol{\xi})}{p(\boldsymbol{q})}. \tag{47}$$

More specifically, the likelihood is defined by the conditional distribution of the data as a function of the parameters $L(\boldsymbol{\xi}|\boldsymbol{q}) = p(\boldsymbol{q}|\boldsymbol{\xi})$, but to emphasize the dependence on the value of the parameters it is often written in the former notation. The denominator in Bayes' Theorem acts as a normalization constant and using the law of total probability can be expressed as,

$$p(\boldsymbol{q}) = \int_{\Xi} p(\boldsymbol{q}|\boldsymbol{\xi}) p(\boldsymbol{\xi}) d\boldsymbol{\xi}. \tag{48}$$

Perhaps the most critical component of the Bayesian framework is the likelihood function. Ideally the likelihood is determined by the measurement process, or any other process contributing to uncertainty in the calibration data. For example, if the measurement error is additive, meaning the observations take the form,

$$\boldsymbol{q} = M(\boldsymbol{\xi}) + \boldsymbol{\epsilon}, \tag{49}$$

where $M(\boldsymbol{\xi})$ is the predicted value of $\boldsymbol{q}$ using the model with parameters $\boldsymbol{\xi}$ and $\boldsymbol{\epsilon} \in \mathbb{R}^n$ is the error model with distribution $p_{\boldsymbol{\epsilon}}$, then the likelihood is given by

$$L(\boldsymbol{\xi}|\boldsymbol{q}) = p_{\boldsymbol{\epsilon}}\left(\boldsymbol{q} - M(\boldsymbol{\xi})\right). \tag{50}$$

In practice, while one might have a decent estimate of the uncertainty in measurements, it is often difficult to fully characterize the distribution of experimental uncertainty. For this reason, it can be beneficial to use a model selection procedure to determine the best choice of uncertainty model.

5.2 Calibration data

Specifically, we use the same calibration data as Oliver and Moser [10], which was obtained from direct numerical simulations by Jaminez et al. [59, 60]. Mean velocity measurements were taken at $Re_\tau = 944$ and $Re_\tau = 2003$. The uncertainty in the observations from the direct simulation is the result of calculating the sample mean rather than the true mean. The authors of [61] provide an estimate of the variance in

the error, however the covariance between data points in the profile is not provided. To minimize the impact of the correlation between measurement points, Oliver and Moser [10] downsample the data and use points that are farther apart; we will do the same and assume the data points are independent.

Since the simulation of the channel flow is dependent on the Reynolds number Re_τ, we will construct two surrogate models, one for each flow scenario. Technically, one could attempt to construct a projection of the mean velocity whose coefficients are dependent on the Reynolds number, in addition to the location in the channel. We choose not to do this here because of the interface required between the channel simulation code and the code used to perform the goal-oriented adaptivity of the surrogate model. This does however increase the computational burden of our approach.

For all error models we will use the same surrogate construction for the approximate forward models.

As we did in the examination of the forward model, we consider six uncertain parameters. This set of parameters is naturally augmented with the calibration parameters for the uncertainty models considered. For both Reynolds numbers we will use the final expansion order in Table 2, $\mathcal{N} = (6, 3, 3, 1, 2, 2)$, which yields error estimates $\eta_{944} = 1.388788 \times 10^{-2}$ and $\eta_{2003} = 1.878746 \times 10^{-2}$.

5.3 Multiplicative error models

We begin with the general description of the model error by supposing that the error is multiplicative in terms of the velocity. Thus, the observed data is taken to be governed by the equation,

$$\langle u \rangle^+ (z;\xi) = (1 + \boldsymbol{\epsilon}(z;\xi))U^+(z;\xi), \tag{51}$$

where $z = y/H$ is the non-dimensionalized wall-normal coordinate, $U^+ = U/u_*$ is the non-dimensionalized velocity, and $\langle u \rangle^+$ is the prediction of the true non-dimensionalized velocity. We assume a zero-mean Gaussian field for the error term $\boldsymbol{\epsilon} = \boldsymbol{\epsilon}(z) = \boldsymbol{\epsilon}(z;\xi)$. The previous studies [52, 10] investigated three different definitions of the covariance of $\boldsymbol{\epsilon}$. Again, to simplify the presentation here we review only one of these choices: a correlated inhomogeneous covariance structure.

Since length scales in turbulent flows are set differently based on the region of the flow, it makes sense to incorporate that structure in the uncertainty model. To mimic the change in length scales, we use a covariance function with a variable length scale [10, 62],

$$\langle \boldsymbol{\epsilon}(z)\boldsymbol{\epsilon}(z') \rangle = \sigma^2 \left(\frac{2l(z)l(z')}{l^2(z) + l^2(z')} \right)^{1/2} \exp\left(-\frac{(z-z')^2}{l^2(z) + l^2(z')} \right), \tag{52}$$

where σ is a calibration parameter and the length scale function $l(z)$ is given by,

$$l(z) = \begin{cases} l_{\text{in}} & \text{for } z < z_{\text{in}} \\ l_{\text{in}} + \frac{l_{\text{out}} - l_{\text{in}}}{z_{\text{out}} - z_{\text{in}}}(z - z_{\text{in}}) & \text{for } z_{\text{in}} \le z \le z_{\text{out}} \\ l_{\text{out}} & \text{for } z > z_{\text{out}}. \end{cases} \tag{53}$$

Here $l_{\text{in}} = l_{\text{in}}^+/Re_\tau$, $z_{\text{in}} = z_{\text{in}}^+/Re_\tau$, and l_{in}^+, z_{in}^+, l_{out}, and z_{out} are additional calibration parameters.

Using the surrogate models to evaluate U^+, and the covariance defined above, the likelihood for the uncertainty model is given by

$$L_{Re_\tau}(\xi|q) = \prod_i^n p_{\epsilon_i}\left(\frac{q_i}{U_i^+(z;\xi)} - 1\right), \tag{54}$$

where $\xi = \{\kappa, c_{b1}, \sigma_{\text{SA}}, c_{b2}, c_{v1}, c_{w2}, \sigma, l_{\text{in}}^+, z_{\text{in}}^+, l_{\text{out}}, z_{\text{out}}\}$. The same uniform distributions used to define the parameter ranges in Section 4.4 are carried over here as the prior distributions for each parameter. Kernel density estimates of the posterior densities resulting from the Bayesian calibration are shown in Figures 3 13. We see excellent agreement between the posteriors obtained from the full model simulation and our surrogate model. Results for the full set of parameters are rather promising. While some minor differences are observed in the posterior distributions, overall the agreement is remarkable. Of particular note is the only minor discrepancies in the most sensitive parameters, κ specifically.

Our results suggest that the surrogate model can in fact be used to calibrate the full model without the need for costly full model evaluations in the process. In fact, some work has been done to show that, in limited cases with mostly Gaussian assumptions, the error in the surrogate model can be used to prove a bound on the error in the posterior distributions obtained through Bayesian inference [2, 3, 5, 4]. However, further effort is needed to extend these results to more general cases.

Unfortunately the computational cost for constructing the surrogate model in this case is on par with the additional cost associated with using the full model directly in the Bayesian framework; making it difficult to argue that one should use the surrogate approach at all. If however, one wishes to perform a model selection procedure, or even just a subsequent analysis with an alternative error model, the cost of constructing the surrogate forward model can be amortized. In [52] a more extensive model selection study shows that that even for relative studies of this nature, the surrogate model described here leads to the same conclusion as using the full model to perform the same analysis.

6 Conclusion

We have examined the application of goal-oriented error estimation to the adaptivity of surrogate models for boundary-value problems with uncertainty. In contrast to existing anisotropic refinement strategies, a new refinement algorithm was proposed that uses higher-order information from the goal-oriented error estimate to identify the most influential parameters and adapt the surrogate model accordingly.

Based on our approach, an accurate surrogate model need to be constructed for the Spalart-Allmaras turbulence model and the solution of the RANS equations in a fully-developed channel. The reduced model was then used in a Bayesian model calibration study in place of the full simulation. Posterior distributions for the parameters showed excellent agreement with those obtained using the original forward model. The results demonstrate that the newly developed methodology can be a valuable resource to computational scientists in assessing complex physical systems using Bayesian techniques where a large number of model simulations are required.

Acknowledgements

Serge Prudhomme is grateful for the support by a Discovery Grant from the Natural Sciences and Engineering Research Council of Canada. He is also a participant of the KAUST SRI Center for Uncertainty Quantification in Computational Science and Engineering. Corey Bryant acknowledges the support by the Department of Energy [National Nuclear Security Administration] under Award Number [DE-FC52-08NA28615].

Author details

[1]Département de Mathématiques et de Génie Industriel, Ecole Polytechnique de Montréal, Montréal, Québec, Canada. [2] Institute for Computational Engineering and Sciences (ICES), The University of Texas at Austin, Austin, TX, USA.

References

1. Kennedy, M.C., O'Hagan, A.: Bayesian calibration of computer models. J. Royal Statist. Soc. Series B **63**(3), 425–464 (2001)
2. Li, J., Marzouk, Y.: Adaptive construction of surrogates for the Bayesian solution of inverse problems. SIAM J. Sci. Comput. **36**, 1164–1186 (2014)
3. Ma, X., Zabaras, N.: An efficient Bayesian inference approach to inverse problems based on an adaptive sparse grid collocation method. Inverse Problems **25**(3), 035013 (2009)
4. Marzouk, Y., Najm, H., Rahn, L.: Stochastic spectral methods for efficient Bayesian solution of inverse problems. J. Comput. Physics **224**, 560–586 (2007)
5. Marzouk, Y., Xiu, D.: A stochastic collocation approach to bayesian inference in inverse problems. Communications in computational physics **6**(4), 826–847 (2009)
6. Oden, J.T., Prudhomme, S.: Estimation of Modeling Error in Computational Mechanics. J. Comput. Physics **182**, 496–515 (2002)
7. Oden, J.T., Prudhomme, S., Romkes, A., Bauman, P.T.: Multiscale Modeling of Physical Phenomena: Adaptive Control of Models. SIAM J. Sci. Comput. **28**(6), 2359 (2006)
8. Allmaras, S.R., Johnson, F.T., Spalart, P.R.: Modifications and clarifications for the implementation of the spalart-allmaras turbulence model. In: Seventh International Conference on Computational Fluid Dynamics (ICCDF7), Big Island, Hawaii, USA, 9-13 July 2012 (2012)
9. Spalart, P.R., Allmaras, S.R.: A one-equation turbulence model for aerodynamic flows. Recherche Aérospatiale (1), 5–21 (1994)
10. Oliver, T.A., Moser, R.D.: Bayesian uncertainty quantification applied to rans turbulence models. Journal of Physics: Conference Series **318**(4), 042032 (2011)
11. Cheung, S.H., Oliver, T.A., Prudencio, E.E., Prudhomme, S., Moser, R.D.: Bayesian uncertainty analysis with applications to turbulence modeling. Reliability Engineering & System Safety **96**(9), 1137–1149 (2011)
12. Durbin, P.A., Petterson Reif, B.A.: Statistical Theory and Modeling for Turbulent Flows. Wiley, New York (2001)
13. Moser, R.D.: Turbulence (Lecture Notes, 2013)
14. Pope, S.B.: Turbulent Flows. Cambridge University Press, New York (2000)
15. Baldwin, B., Lomax, H.: Thin-layer approximation and algebraic model for separated turbulent flows. AIAA Paper **257** (1978)
16. Chien, K.Y.: Predictions of channel and boundary-layer flows with a low-Reynolds-number two-equation model of turbulence. AIAA Journal **20**(1), 33–38 (1982)
17. Durbin, P.A.: Separated flow computations with the $k-\epsilon-v^2$ model. AIAA Journal **33**, 659–664 (1995). doi:10.2514/3.12628
18. Oliver, T.A., Darmofal, D.L.: Impact of turbulence model irregularity on high-order discretizations. AIAA Paper **953** (2009)
19. Ghanem, R., Red-Horse, J.: Propagation of probabilistic uncertainty in complex physical systems using a stochastic finite element approach. Physica D: Nonlinear Phenomena **133**, 137–144 (1999)
20. Ghanem, R., Spanos, P.: Stochastic Finite Elements: A Spectral Approach. Springer, New York (2002)
21. Xiu, D., Karniadakis, G.: The Wiener-Askey polynomial chaos for stochastic differential equations. SIAM J. Sci. Comput. **24**, 619–644 (2002)
22. Wan, X., Karniadakis, G.E.: An adaptive multi-element generalized polynomial chaos method for stochastic differential equations. J. Comput. Phys. **209(2)**, 617–642 (2005)
23. Wan, X., Karniadakis, G.: Solving elliptic problems with non-Gaussian spatially-dependent random coefficients. Computer Methods in Applied Mechanics and Engineering **198**(21-26), 1985–1995 (2009)
24. Wan, X., Karniadakis, G.: Error control in multi-element generalized polynomial chaos method for elliptic problems with random coefficients. Communications in Computational Physics **5**(2-4), 793–820 (2009)
25. Constantine, P.G., Eldred, M.S., Phipps, E.T.: Sparse pseudospectral approximation method. Computer Methods in Applied Mechanics and Engineering **229-232**, 1–12 (2012)
26. Gautschi, W.: Orthogonal polynomials: applications and computation. Acta Numerica **5**, 45–119 (1996)
27. Gautschi, W.: Orthogonal Polynomials: Computation and Approximation. Clarendon Press, Oxford (2004)
28. Dunkl, C.F., Xu, Y.: Orthogonal Polynomials in Several Variables. Cambridge University Press, New York (2001)
29. Cameron, R., Martin, W.: The orthogonal development of non-linear functionals in series of Fourier-Hermite functionals. Annals of Mathematics **48**, 385–392 (1947)
30. Ernst, O.G., Mugler, A., Starkloff, H.-J., Ullmann, E.: On the convergence of generalized polynomial chaos expansions. ESAIM: Mathematical Modelling and Numerical Analysis **46**(2), 317–339 (2011). doi:10.1051/m2an/2011045
31. Le Maître, O., Knio, O.: Spectral Methods for Uncertainty Quantification: With Applications to Computational Fluid Dynamics. Springer, New York (2010)

32. Butler, T., Dawson, C., Wildey, T.: A posteriori error analysis of stochastic spectral methods. SIAM J. Sci. Comput. **33**, 1267–1291 (2011)
33. Butler, T., Constantine, P., Wildey, T.: A posteriori error analysis of parameterized linear systems using spectral methods. SIAM. J. Matrix Anal. Appl. **33**, 195–209 (2012)
34. Babuška, I., Nobile, F., Tempone, R.: A stochastic collocation method for elliptic partial differential equations with random input data. SIAM J. Numer. Anal. **45**(3), 1005–1034 (2007)
35. Ganis, B., Klie, H., Wheeler, M.F., Wildey, T., Yotov, I., Zhang, D.: Stochastic collocation and mixed finite elements for flow in porous media. Comput. Methods Appl. Mech. Engrg **197**(43-44), 3547–3559 (2008)
36. Gerstner, T., Griebel, M.: Dimension-adaptive tensor-product quadrature. Computing **71**(1), 65–87 (2003)
37. Nobile, F., Tempone, R., Webster, C.G.: An anisotropic sparse grid stochastic collocation method for partial differential equations with random input data. Siam J. Numer. Anal **46**(5), 2411–2442 (2008)
38. Nobile, F., Tempone, R., Webster, C.G.: A sparse grid stochastic collocation method for partial differential equations with random input data. Siam J. Numer. Anal **46**(5), 2309–2345 (2008)
39. Todor, R.A., Schwab, C.: Convergence rates for sparse chaos approximations of elliptic problems with stochastic coefficients. IMA Journal of Numerical Analysis **27**(2), 232–261 (2006)
40. Constantine, P.G., Gleich, D.F., Iaccarino, G.: Spectral methods for parameterized matrix equations. SIAM. J. Matrix Anal. Appl. **31**, 2681–2699 (2010)
41. Almeida, R.C., Oden, J.T.: Solution verification, goal-oriented adaptive methods for stochastic advection-diffusion problems. Comput. Methods Appl. Mech. Eng. **199**(37-40), 2472–2486 (2010). doi:10.1016/j.cma.2010.04.001
42. Bryant, C.M., Prudhomme, S., Wildey, T.: A posteriori error control for partial differential equations with random data. ICES Report 13-08 (2013)
43. Bryant, C.M., Prudhomme, S., Wildey, T.: Error decomposition and adaptivity for response surface approximations from pdes with parametric uncertainty. Submitted to SIAM/ASA J. Uncert. Quant. (2014)
44. Mathelin, L., Le Maître, O.: Dual-based a posteriori error estimate for stochastic finite element methods. Communications in Applied Mathematics and Computational Science **2**(1), 83–115 (2007). doi:10.2140/camcos.2007.2.83
45. Eriksson, K., Estep, D., Hansbo, P., Johnson, C.: Introduction to adaptive methods for differential equations. Acta Numer., 105–158 (1995)
46. Eriksson, K., Estep, D., Hansbo, P., Johnson, C.: Computational Differential Equations. Cambridge University Press, New York (1996)
47. Becker, R., Rannacher, R.: An optimal control approach to a posteriori error estimation in finite element methods. Acta Numer. **10**, 1–102 (2001)
48. Oden, J.T., Prudhomme, S.: Goal-oriented error estimation and adaptivity for the finite element method. Computers & Mathematics with Applications **41**(5), 735–756 (2001)
49. Ainsworth, M., Oden, J.T.: A Posteriori Error Estimation in Finite Element Analysis. John Wiley & Sons, New York (2000)
50. Babuška, I., Strouboulis, T.: The Finite Element Method and Its Reliability. Oxford University Press, Oxford (2001)
51. Verfürth, R.: A Posteriori Error Estimation Techniques for Finite Element Methods. Numerical Mathematics and Scientific Computation. Oxford University Press, New York (2013)
52. Bryant, C.M.: On goal-oriented error estimation and adaptivity for nonlinear systems with uncertain data and application to flow problems. PhD thesis, The University of Texas at Austin, Austin, TX. (2014)
53. van der Zee, K.G.: Goal-adaptive discretization of fluid-structure interaction. PhD thesis, Delft University of Technology, The Netherlands (2009)
54. Bangerth, W., Rannacher, R.: Adaptive Finite Element Methods for Differential Equations. Birkhauser Verlag, Boston (2003)
55. Estep, D., Larson, M.G., Williams, R.D.: Estimating the Error of Numerical Solutions of Systems of Reaction-diffusion Equations. American Mathematical Soc., Providence (2000)
56. Ma, X., Zabaras, N.: An adaptive hierarchical sparse grid collocation algorithm for the solution of stochastic differential equations. J. Comput. Phys. **228**(8), 3084–3113 (2009). doi:10.1016/j.jcp.2009.01.006
57. Calvetti, D., Somersalo, E.: Introduction to Bayesian Scientific Computing. Springer, New York (2007)
58. Kaipio, J., Somersalo, E.: Statistical and Computational Inverse Problems. Springer, New York (2005)
59. Hoyas, S., Jiménez, J.: Scaling of the velocity fluctuations in turbulent channels up to $Re_\tau = 2003$. Physics of Fluids **18**(1), 011702 (2006)
60. Del Alamo, J.C., Jiménez, J., Zandonade, P., Moser, R.D.: Scaling of the energy spectra of turbulent channels. Journal of Fluid Mechanics **500**, 135–144 (2004)
61. Hoyas, S., Jiménez, J.: Reynolds number effects on the Reynolds-stress budgets in turbulent channels. Physics of Fluids **20**(10), 101511 (2008)
62. Rasmussen, C.E., Williams, K.I.: Gaussian Processes for Machine Learning. MIT Press, Cambridge (2006)

Figures

Tables

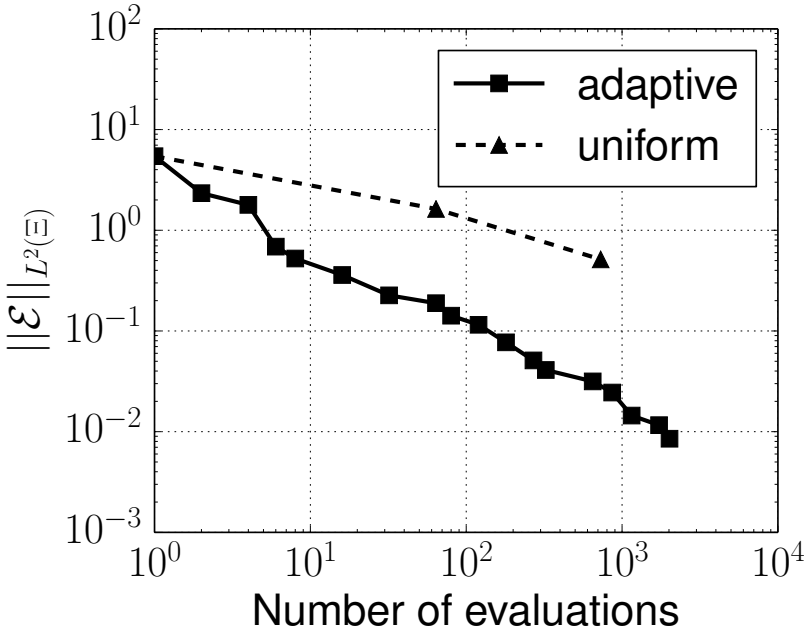

Figure 1 Convergence of error estimate for adaptive surrogate of Spalart-Allmaras turbulence model with six uncertain parameters.

Table 1 Standard parameter values for the Spalart-Allmaras turbulence model [10].

Parameter	Standard value
c_{b1}	0.1355
σ_{SA}	2/3
c_{b2}	0.622
κ	0.41
c_{w2}	0.3
c_{w3}	2
c_{v1}	7.1
c_{v2}	0.7
c_{v3}	0.9

Table 2 Expansion orders for parameters in adaptive surrogate of Spalart-Allmaras turbulence model.

iteration	κ	c_{b1}	σ_{SA}	c_{b2}	c_{v1}	c_{w2}
1	0	0	0	0	0	0
2	1	0	0	0	0	0
3	1	0	0	0	1	0
4	2	0	0	0	1	0
5	3	0	0	0	1	0
6	3	0	1	0	1	0
7	3	1	1	0	1	0
8	3	1	1	0	1	1
9	4	1	1	0	1	1
10	4	2	1	0	1	1
11	4	2	2	0	1	1
12	4	2	2	0	2	1
13	5	2	2	0	2	1
14	5	2	2	1	2	1
15	5	2	3	1	2	1
16	5	3	3	1	2	1
17	5	3	3	1	2	2
18	6	3	3	1	2	2

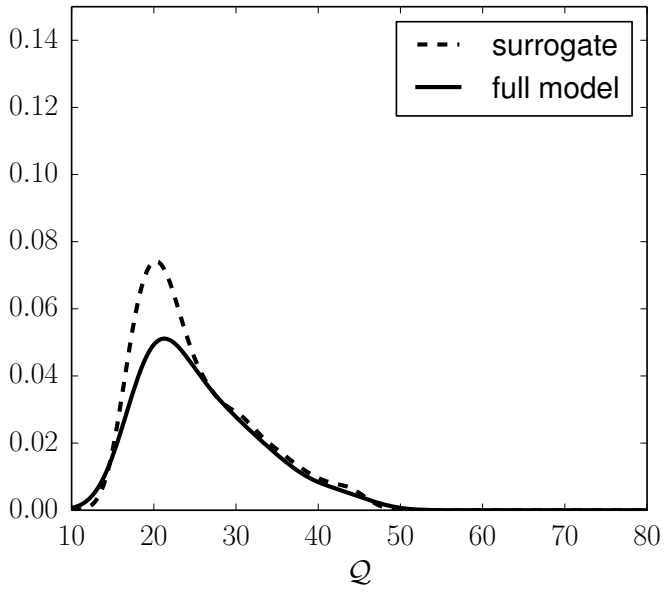

Figure 2 Kernel density estimates of the average velocity from the six-parameter Spalart-Allmaras turbulence model.

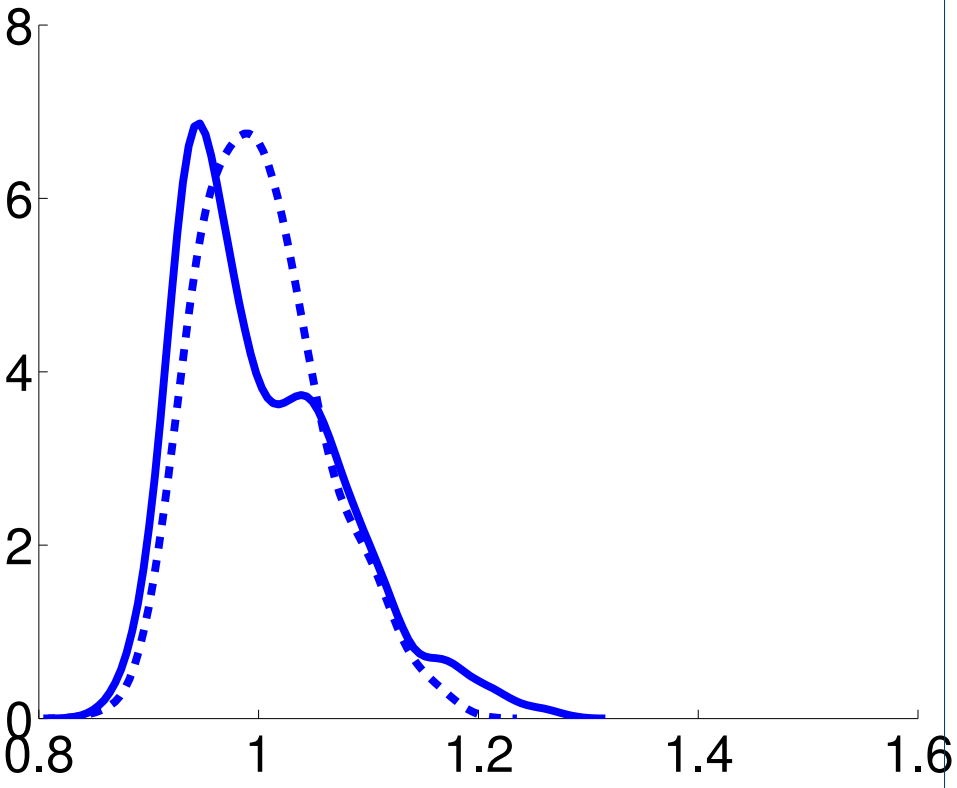

Figure 3 Posterior probability density for κ. Full model (solid line) and surrogate model (dashed), where 1 indicates nominal value.

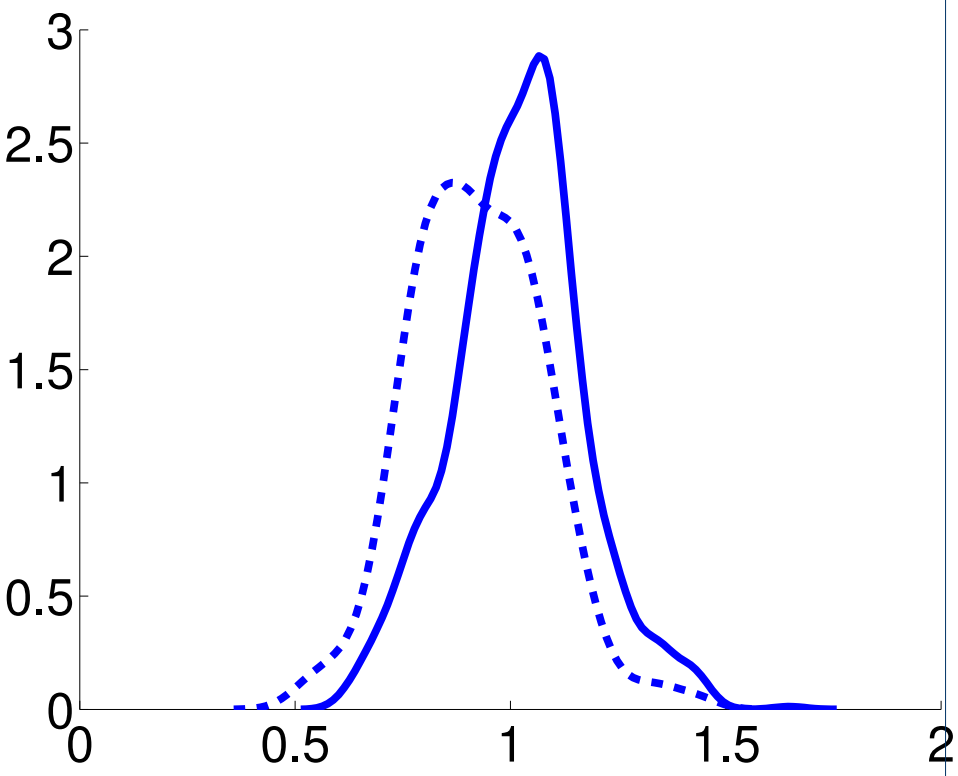

Figure 4 Posterior probability density for c_{b1}. Full model (solid line) and surrogate model (dashed), where 1 indicates nominal value.

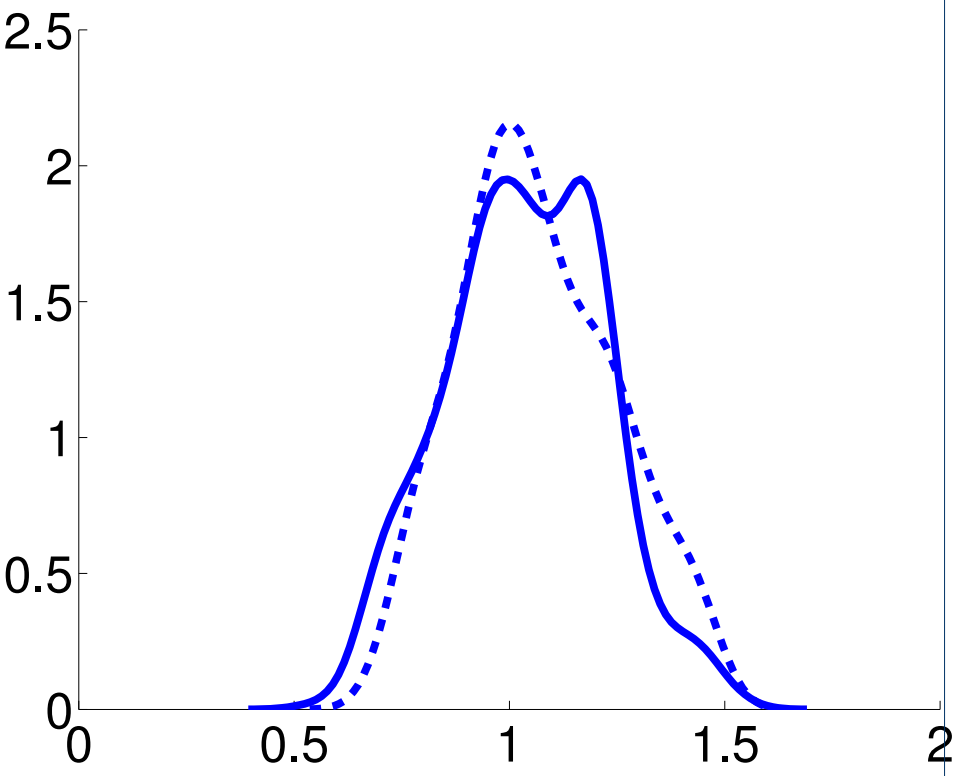

Figure 5 Posterior probability density for σ_{SA}. Full model (solid line) and surrogate model (dashed), where 1 indicates nominal value.

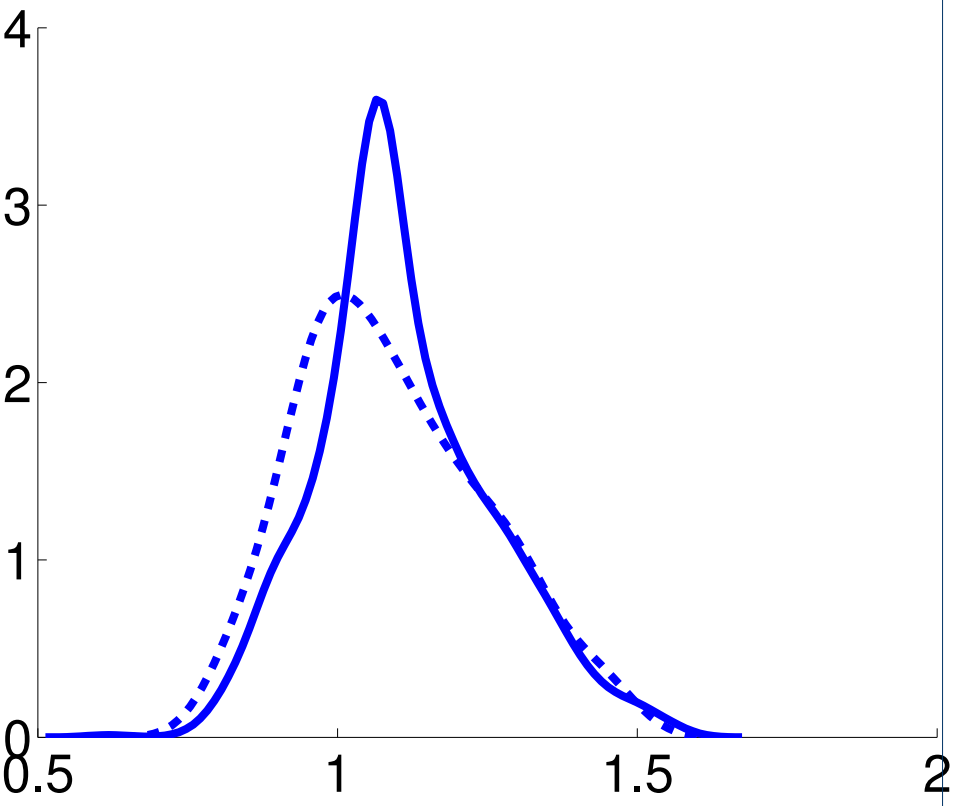

Figure 6 Posterior probability density for c_{b2}. Full model (solid line) and surrogate model (dashed), where 1 indicates nominal value.

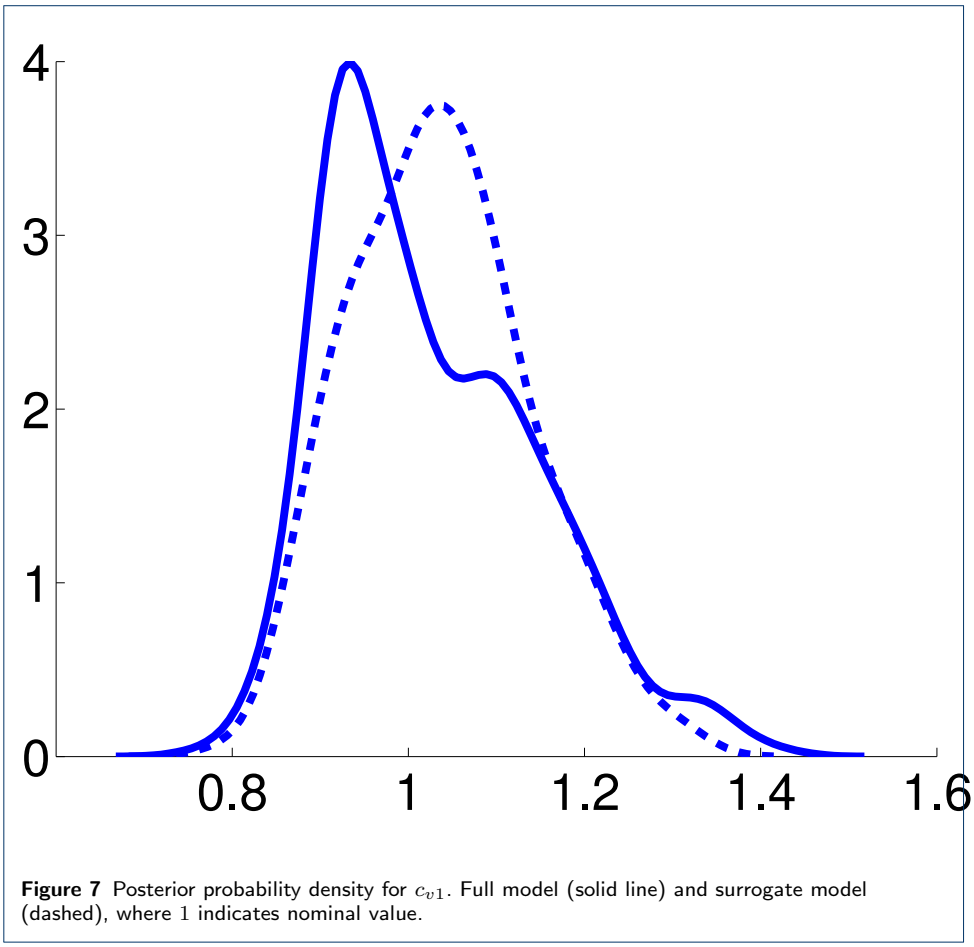

Figure 7 Posterior probability density for c_{v1}. Full model (solid line) and surrogate model (dashed), where 1 indicates nominal value.

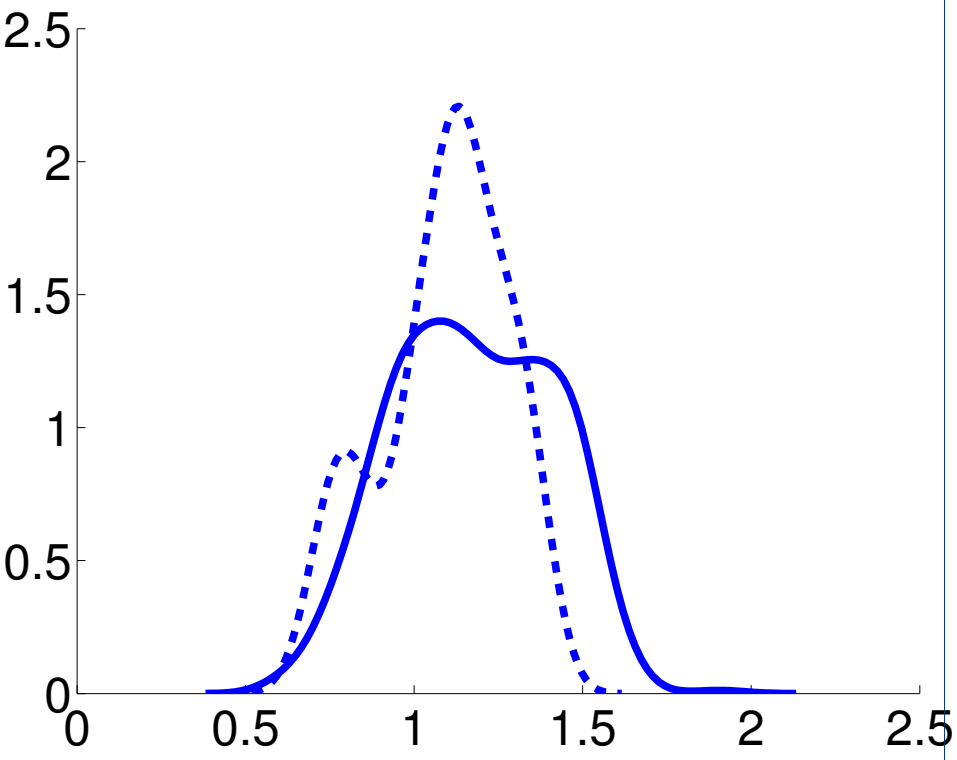

Figure 8 Posterior probability density for c_{w2}. Full model (solid line) and surrogate model (dashed), where 1 indicates nominal value.

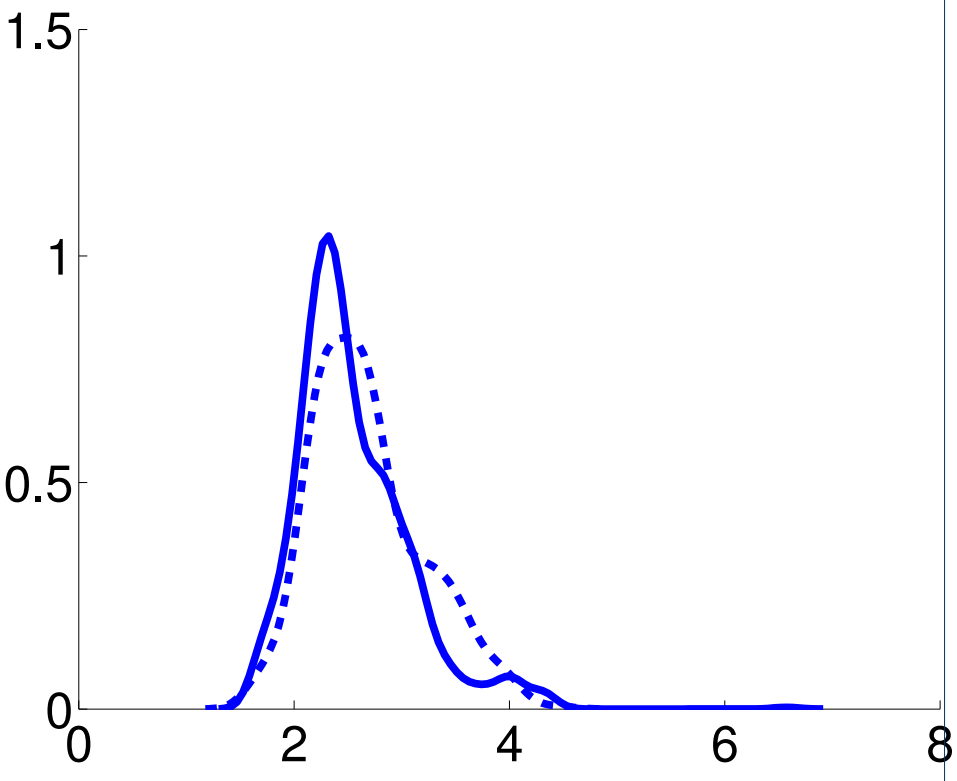

Figure 9 Posterior probability density for σ. Full model (solid line) and surrogate model (dashed), where 1 indicates nominal value.

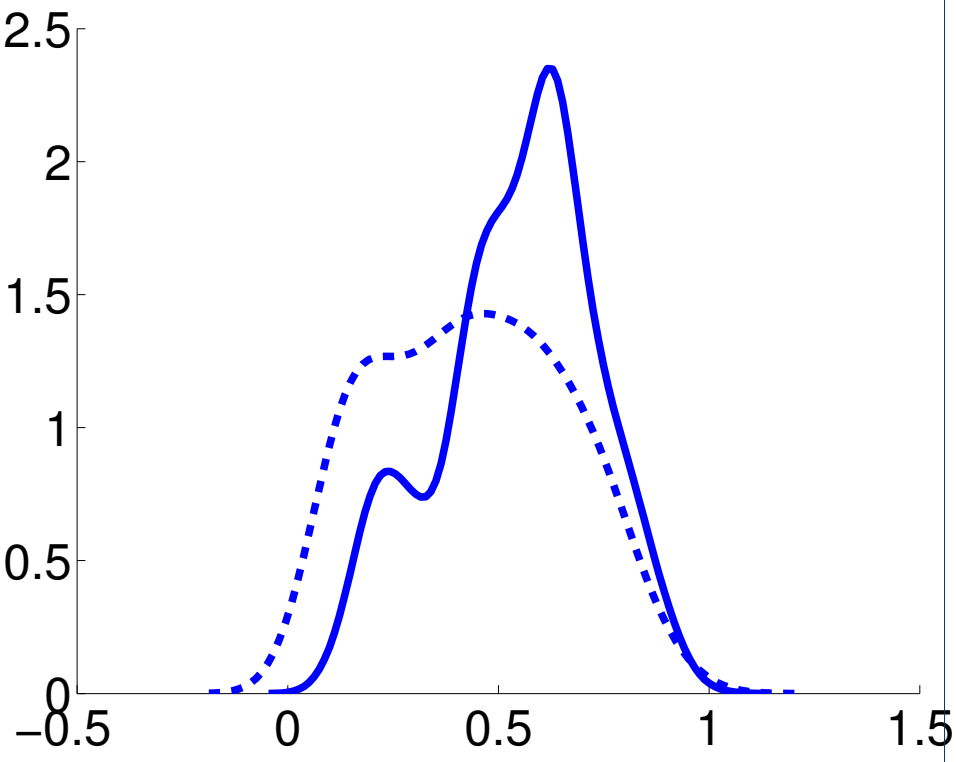

Figure 10 Posterior probability density for l_{in}^{+}. Full model (solid line) and surrogate model (dashed), where 1 indicates nominal value.

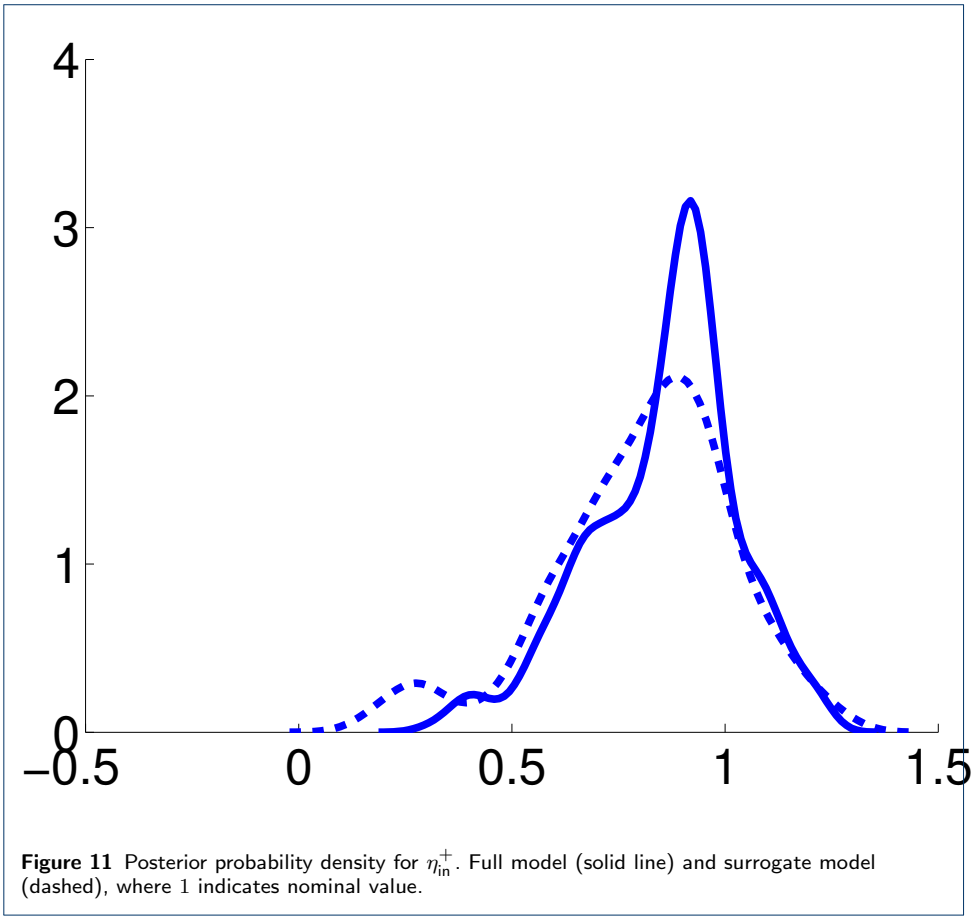

Figure 11 Posterior probability density for η_{in}^{+}. Full model (solid line) and surrogate model (dashed), where 1 indicates nominal value.

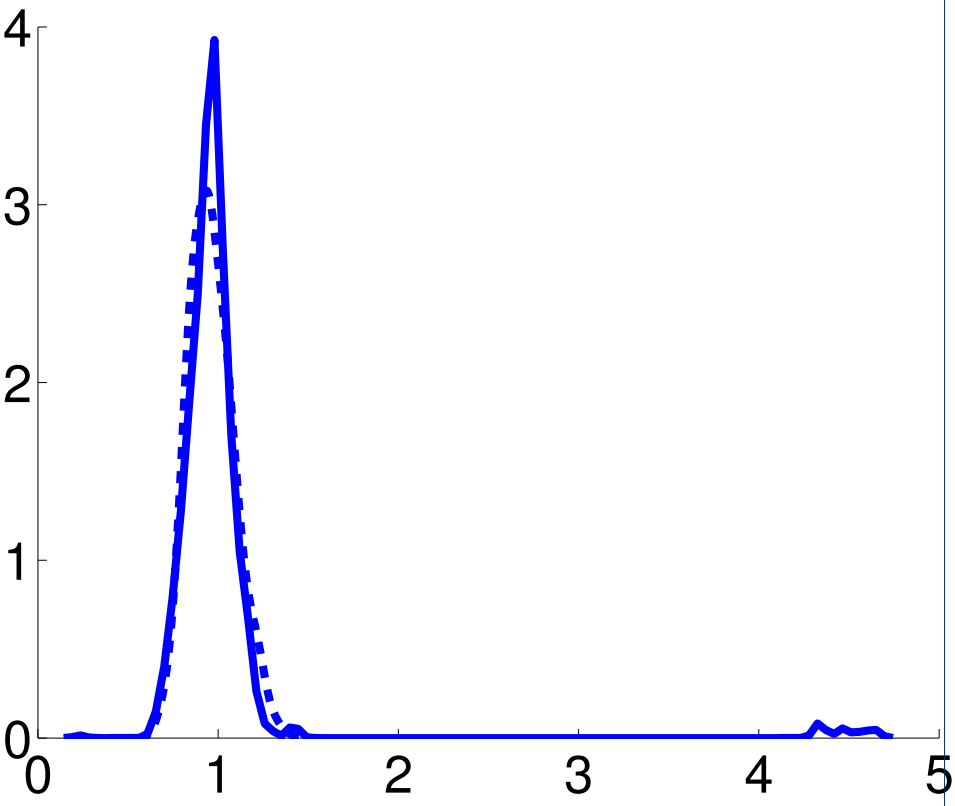

Figure 12 Posterior probability density for η_{out}. Full model (solid line) and surrogate model (dashed), where 1 indicates nominal value.

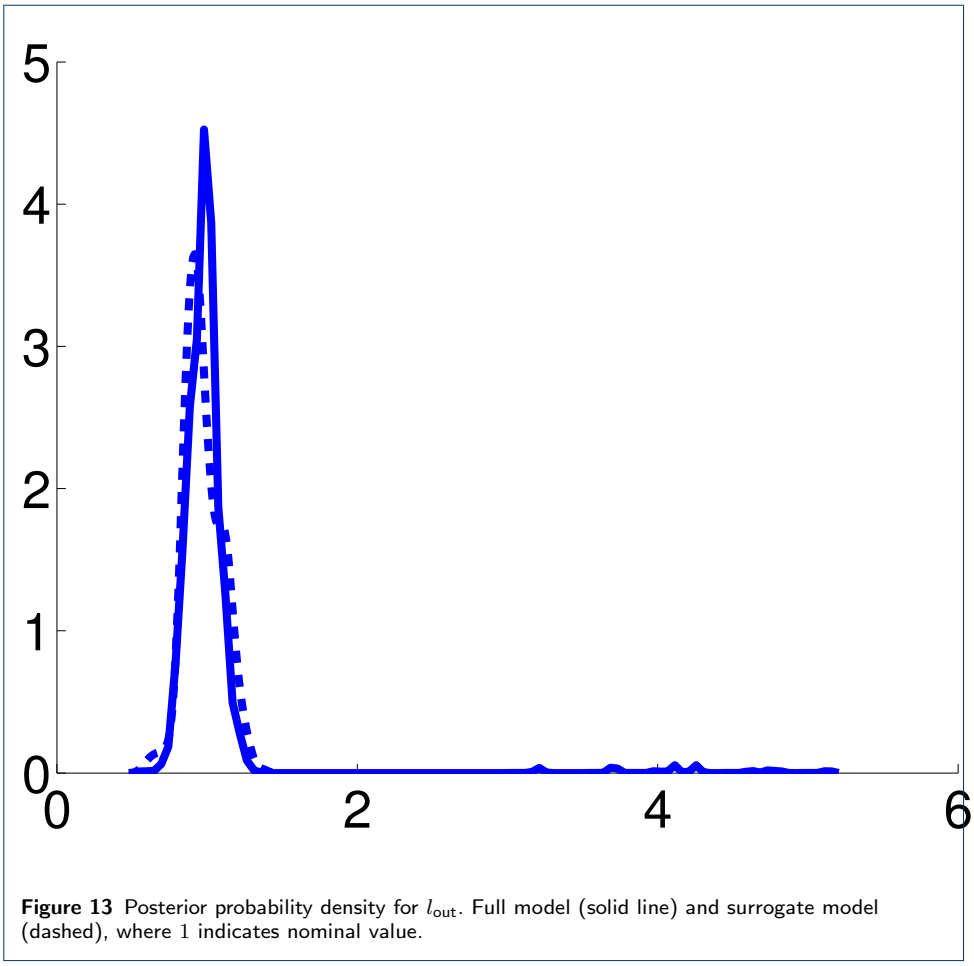

Figure 13 Posterior probability density for l_{out}. Full model (solid line) and surrogate model (dashed), where 1 indicates nominal value.